Elevated Temperature Nanoindentation Creep Study of Plastically Deformed and Spark Plasma Sintered UO_2

David Frazer , Benjamin Shaffer , Bowen Gong , Pedro Peralta , Jie Lian , Peter Hosemann

PII: S0022-3115(20)31213-7
DOI: https://doi.org/10.1016/j.jnucmat.2020.152605
Reference: NUMA 152605

To appear in: *Journal of Nuclear Materials*

Received date: 2 July 2020
Revised date: 10 October 2020
Accepted date: 15 October 2020

Please cite this article as: David Frazer , Benjamin Shaffer , Bowen Gong , Pedro Peralta , Jie Lian , Peter Hosemann , Elevated Temperature Nanoindentation Creep Study of Plastically Deformed and Spark Plasma Sintered UO_2, *Journal of Nuclear Materials* (2020), doi: https://doi.org/10.1016/j.jnucmat.2020.152605

Elevated Temperature Nanoindentation Creep Study of Plastically Deformed and Spark Plasma Sintered UO_2

David Frazer[a,b], Benjamin Shaffer[c], Bowen Gong[d], Pedro Peralta[c], Jie Lian[d], and Peter Hosemann[a, e]

[a] Nuclear Engineering Department, University of California, Berkeley, 4153 Etcheverry Hall Berkeley, Ca

[b] Idaho National Laboratory, Materials and Fuels Complex, 2525 Fremont Ave, Idaho Falls, ID USA

[c] School for Engineering of Matter, Transport, and Energy, Arizona State University, Tempe, AZ 85287, United States

[d] Department of Mechanical, Aerospace, Nuclear Engineering, Rensselaer Polytechnic Institute, Troy, NY, 12180

[e] Lawrence Berkeley National Laboratory, Material Science division, Berkeley, CA

Abstract

Current challenges with uranium dioxide fuel degradation include fuel swelling, cracking and fission gas release, all of which reduce the operational life span of the fuel in commercial reactors. One important factor in prolonging the life span of uranium dioxide (UO_2) fuel is developing a good understanding of the mechanical properties of the high burnup structure that forms at the periphery of the fuel pellet during the fuel cycle. Nanoindentation based testing techniques can probe the mechanical properties of small volumes of material and measure properties including hardness, elastic modulus, and creep. In this work, elevated temperature nanoindentation and nanoindentation creep testing is performed on UO_2 samples with different microstructures, including nanocrystalline (NC) grains, as well as microcrystalline samples with different grain sizes and creep prestrains introduced at high temperatures. Tests allowed measuring hardness, elastic modulus and creep stress exponents up to 500 °C. The test results indicate that for temperatures and stresses used here, NC UO_2 had limited to no creep, with stress exponents greater than 10. For UO_2 samples with creep prestrain and spark plasma sintered (SPS) UO_2 with a 1.8 μm grain size the dominant creep mechanism at the high stresses and relatively low temperatures used is dislocation glide: the creep stress exponents of 3-4 at 500 °C also matched well with recent literature values for macro scale compression creep tests. In addition, it was observed that the UO_2 samples containing higher dislocation defect densities had lower creep stress exponents than conventional sintered UO_2. The stress exponent measured on the conventional sintered UO_2 at 500 °C was ~ 7, which suggests that the deformation of UO_2 at lower temperatures might be hindered by the energetic barriers to dislocation nucleation.

Keywords: Nanoindentation Creep, High Temperature Nanoindentation, Uranium Dioxide

Introduction

Uranium dioxide (UO_2) is the standard fuel of today's nuclear reactor fleet and a potential fuel for some generation IV reactors [1]. Pellet cladding mechanical interactions (PMCI) can lead to cladding failures resulting in the release of radioactive material [2-5]. A better understanding of the mechanical behavior of UO_2 fuel at its operational temperature in the reactor would

contribute to better modeling of PMCI. In commercial light water reactors (LWRs), the majority of the pellets operate below 1000 ºC [2-5] and the pellet periphery that contacts the cladding material is approximately at 500 ºC. While some mechanical testing in the temperature range of less than 1000 ºC has been performed [6-17], creep has not been thoroughly investigated in UO_2 at these intermediate temperatures. However, numerous studies at temperatures greater than 1000 ºC [18-25] have been conducted. This study investigates creep in the intermediate temperature regime, which is highly relevant to developing a better understanding of commercial fuel pellet performance in LWR applications. During the entire duration of their service period, when the fuel is being used in reactor operation, UO_2 pellets undergo a variety of microstructural evolutions that affect the local properties of the pellet [1]. As fuel is used, the high burnup structure (HBS) forms at the pellet's periphery and is characterized by a nanocrystalline grain size and high porosity [26-28]. The mechanical properties of the HBS is important for PCMI because it represents the microstructure of the region of the pellet that is in contact with the cladding and a crack in the fuel can initiate a crack in the cladding. Evaluating this microstructure is difficult because the actual fuel is highly radioactive making it difficult to work with.

With new sintering techniques such as spark plasma sintering (SPS), it is possible to produce dense UO_2 samples with a nanocrystalline microstructure for characterizing its mechanical properties [29, 30]. These SPS specimens with nanometer-size grains allow surrogate testing of the HBS without using actual spent, highly radioactive fuel samples and difficult sample preparations.

Instrumented indentation-based techniques can be used to evaluate the mechanical properties of small pieces or local areas of SPS samples. These techniques can measure the hardness, elastic modulus and creep exponents of materials. In this research, these techniques are used on fresh samples of UO_2 with the expectation that the results could be utilized to design further experiments for spent fuel and to produce useful comparisons. Nanoindentation can be used to study the localized nanoindentation creep of the sample in an analogous way to impression creep testing [31]. In addition, nanoindentation creep testing is a useful tool for investigating the creep behavior of materials due to the short testing duration and limited sample size requirements [32]. Furthermore, other research confirms that the activation energy and stress exponents calculated from nanoindentation creep match well with uniaxial creep test results [31-36]. However, there are still several experimental and modeling challenges that pose obstacles to direct comparisons of indentation and uniaxial creep results [32, 33]

In this manuscript low and intermediate temperature (room-500 °C) nanoindentation and nanoindentation creep tests were performed on 4 different samples of UO_2. Two samples were conventionally sintered UO_2 with and without pre-straining, while two samples were SPS sintered specimens with1.8 μm and 125 nm grain size (referred to as SPS-1.8 and SPS-125 hereinafter).

Experimental

Sample 1 (sintered) was synthesized at Los Alamos National Laboratory (LANL) using d-UO_2 powder with no additives and no milling prior to pressing. 0.4994g of as-received powder was pressed at 80 MPa (dwell time 60 s) to form a green pellet with diameter 5.71 mm, length 3.96 mm, and density 4.925 g/cc (44.93%TD). The pellet was then partially sintered at 800 °C under 10 CPM wet argon for 5 minutes, resulting in a permeable/porous pellet of mass 0.4980g,

diameter 5.69 mm, length 3.97 mm, density 4.93 g/cc (45.01%TD). This pellet was later sectioned into slices (1.60 mm thick), with one slice (12571-1) heat treated at 1700 °C under 1 SCFH 79% argon/21% oxygen for 35 minutes to complete the sintering process while growing large grains. The disk was then sectioned again, polished, and characterized prior to testing. One half become sample 1 with a 10 μm grain size. The other half became sample 2 and had a standard uniaxial compression creep test performed on it at Arizona State University (ASU). The creep test was performed at 1200 °C in an atmosphere of 95% UHP Ar-5% H_2 for approximately six hours, using an applied load of 471.4 N (106 lbf) for a resulting stress of 180 MPa; the observed steady-state strain rate was 2.07 x 10^{-7} s^{-1}, corresponding to stage II creep, and the sample had a total strain of 9%.

The reason for the pre-straining is that during their deployment in a reactor, commercial fuel pellets will undergo deformation and irradiation damage that produces defects in the fuel pellets that can affect their deformation and mechanical properties including creep [37, 38]. Samples 3 and 4 were SPS produced with a 1.8 μm and 125 nm grain size, respectively. This innovative consolidation technique gains more interest due to its fast process in recent times. The pellets with a grain size of 1.8 μm were sintered from nanocrystalline $UO_{2.03}$ powders at 1300 °C for 30 minutes under a pressure of 40 MPa as described in [29]. Due to the graphite die used in the sintering route, the pellets were reduced in-situ to be hypo-stoichiometric with a final O/M of 1.996 ± 0.004. The pellets with a grain size of 125 nm were sintered at 700 °C for 5 minutes under a pressure of 500 MPa in a WC die. The densified NC pellets were hyper-stoichiometric and a post-sintering annealing was conducted in a tube furnace in 4% H_2/Ar gas atmosphere. Prior to reducing, the furnace was purged for 4 h using a gas flow at a rate of 200 ml/min. The reducing was conducted at 600 °C for 24 h at a gas flow rate of 50 ml/min to produce a stoichiometry of $UO_{2.006}$ in the pellets [29].

The nanoindentation and nanoindentation creep tests were performed with a MicroMaterials Platform 3 indenter with a cubic boron nitride (cBN) Berkovich tip. The procedure for performing these tests was as follows: the samples were mounted onto the hot stage of the MicroMaterials indenter using Omega 700 cement and allowed to cure for 24 hours. During the curing process the high temperature tip was installed on the MicroMaterials indenter and the calibrations for the tip were performed. After the curing process the hot stage was mounted onto the MicroMaterials indenter and room temperature indents were performed. The MicroMaterial's indenter has an environmental chamber that allowed the use of a cover gas for high temperature indentation to inhibit the oxidation of the sample. After the room temperature indents were completed, ultra-high purity (UHP) argon gas was flowed into the environmental chamber at 10 liters/min for 12-18 hours to displace the oxygen in the chamber. The gas was switched to argon+5%H_2 at 6 liters/min and the samples were heated to the desired testing temperature. This mixture of gases has been proven to inhibit the oxidation of other oxygen sensitive samples [29, 39]. Even with the reducing atmosphere, it is believed that the stoichiometry of the UO_2 samples is unchanged during testing due to the low temperature used in these experiments. After reaching the desired testing temperature, there was a 30-60 minute thermal stabilization period. After the stabilization period a test indent was performed to measure the thermal drift between the tip and the sample. The MicroMaterials indenter heats the tip and sample separately giving low thermal drift rates even at high temperature. If the drift during the test indent was excessive (> ± 0.15 nm/s) the sample temperature was adjusted, and then another indentation was performed. This process was repeated until the measured thermal drift post indentation was less than ± 0.15 nm/s.

The indents were carried out in load control mode, by first moving the sample slowly towards the indenter tip until contact was made and then the indenter was slightly retracted. Next the sample was moved until the tip was aligned with the predetermined testing location. The tip was then positioned 1 µm from the sample surface and held there for a 5-minute thermal stabilization period. After this thermal stabilization period the indent was performed. For the nanoindentation experiments the dwell at max load was varied depending on the temperature so the unloading of the indenter was in a steady state condition and did not have unsteady viscoplastic deformation affecting the results. The dwell for room temperature indents was 5-10 seconds, the dwell for the 300 °C was 45 seconds and the dwell for the 500 °C indents was 60 seconds. In the nanoindentation creep experiments the dwell at max load was held for 300 seconds at a load of 100 mN for all of the samples.

Nanoindentation was performed at room temperature (RT), 100°, 300° and 500 ºC on the sintered and pre-strained samples and nanoindentation creep experiments were performed at 300 ºC and 500 ºC on all 4 samples.

Results

The Oliver and Pharr method was used to measure the hardness and reduced modulus of the sintered and pre-strained samples from the nanoindentation experiments [40]. The elastic modulus was calculated from the reduced modulus using the appropriate equation in [40] and the values of elastic modulus of cBN tip material corrected for temperature. The nanoindentation results for sintered and pre-strained samples are displayed in Figure 1. The results of these samples agree well with other high temperature nanoindentation experiments on UO_2 [29].

Figure 2 shows a plot with the difference in the hardness values measured during the nanoindentation experiments and the nanoindentation creep experiments. The nanoindentation values for the SPS-1.8 and SPS-125 samples are from [29] and there is no 500 °C indentation value to compare too. However, there is 600 °C data [29] that can be used for the comparison. This data indicated that for the sintered, pre-strained and SPS-1.8 samples, the hardness value from the nanoindentation creep testing is lower than the nanoindentation hardness measured. The 300 °C testing results for the SPS-125 sample also indicate that the nanoindentation and nanoindentation creep hardness values were approximately the same.

The stress exponent of a nanoindentation creep experiment is calculated from the slope of ln(strain rate) and the ln(stress or hardness) curve [31-36]. This originates from the power-law creep equation for conventional steady-state creep which is shown in equation 1.

$$\dot{\varepsilon} = A\sigma^n \qquad \text{Eq. 1}$$

Where n is the uniaxial stress exponent and A is the uniaxial pre-exponential term, $\dot{\varepsilon}$ is the steady state strain rate, and σ is the stress for a uniaxial creep test.

The strain rate for nanoindentation creep experiments can be calculated with equation 2 [31-36]:

$$\dot{\varepsilon}_i = \left(\frac{1}{h}\right)\left(\frac{dh}{dt}\right) \qquad \text{Eq. 2}$$

Where h is the depth of the indent and dh/dt is the penetration rate in the steady state section or linear portion of the nanoindentation creep curve [31-36], which is assumed to correspond to secondary or steady state creep [31-36]. The stress during nanoindentation creep was calculated

from the area of the tip and the force from the indenter which is the hardness or mean pressure on the sample. The stress exponents for the four nanoindentation creep experiments are shown in Table 1. The plot in Figure 3 presents the typical dwell load, the displacement versus time at the max load, and the change in the measured hardness because of the increase in displacement for the nanoindentation creep experiments. Figure 4 shows representative creep curves, i.e., displacement versus time, for the different samples at the temperatures tested. Lastly, Figures 5 and 6 are representative ln(strain rate) versus ln(stress) curves for the samples tested, along with equations for least square linear fits and the corresponding coefficient of determination R^2.

Discussion

Nanoindentation Hardness

The nanoindentation results demonstrate that the pre-strained sample has a lower hardness value at all testing temperatures compared to the sintered sample (Figure 1), and the difference is larger than the error bars for the measurements. This result agrees with [7], which proposes that the plasticity in UO_2 at lower temperatures might be hindered by the energetic barriers to dislocation nucleation. The authors believe that additional dislocations introduced into the pre-strained samples from the deformation process at elevated temperatures caused the decrease in the hardness [41-43]. Note, however, that there is anisotropy in the elastic modulus and hardness measured in UO_2, and this could play a role in the results, since nanoindentation was used and the length scales involved are such that indent would take place in individual grains for all cases except from the SPS-125 sample due to its nanoscale grain size. In this regard, results from [44] indicate that Knoop hardness testing on single crystals measured a potential 20 % difference in hardness between the lowest and highest measured values. For the 300 ° C case the value of hardness for the pre-strained sample is 4.26 GPa while the value for the sintered sample is 6.04 GPa. If the hardness of the pre-strained sample were to increase by 20 %, as a worst case scenario, it would give a value of 5.11 GPa, which still does not bring the value within one standard deviation of the measured value for the sintered sample. In addition, the experiments here had a minimum of 15 indents at each testing condition and separated by at least 20 μm. The separation distance is larger than the grain size in the material and therefore will measure a random assortment of grains, leading to an average over different orientations.

This would imply that the increased hardness in the sintered sample relative to the pre-strained sample is because dislocations need to nucleate for the deformation to occur in the former, but not in the latter. The pre-straining would increase the initial density of dislocations in the material and therefore not as many dislocations would need to be nucleated for the plastic deformation to occur. It has been documented that irradiated UO_2 develops an initial increase in the hardness of the material after irradiation, but when larger doses are reached there is a reduction in the hardness of the UO_2 [38]. This agrees with the results of this work since the pre-strained sample must have a higher dislocation density compared with sintered sample. While fission and neutron damage would not cause the same damage in UO_2 as a compressive load, the results do show that the presence of additional defects in the UO_2 sample correlate with the reduction in the hardness.

The decrease in hardness between the sintered sample and pre-strained sample was 12 %, 19 %, 29 % and 12 % for RT, 100 ºC, 300 ºC, and 500 ºC respectively. The highest percentage decrease in the hardness was at 300 °C, which is just below the potential ductile to brittle transition range 350-478 ºC for UO_2 [7]. It would suggest that the thermal assistance at 300 ºC is not enough to

allow easy nucleation of dislocations in UO_2 while at the same time dislocation mobility is already efficient. The reduction in the percentage decrease at 500 ºC is because the dislocations are more easily nucleated when the temperature is above the ductile to brittle transition range. The reduction for room temperature and 100 ºC was not as large as 300 ºC because it required higher stress to move the dislocations as they did not have as much thermal assistance.

Figure 2 and Table 2 show a comparison of the nanoindentation hardness and nanoindentation creep hardness of the 4 samples. Unfortunately, due to experimental difficulties there is no 500 °C nanoindentation hardness data for a comparison with the SPS-1.8 and SPS-125 samples. The nanoindentation hardness data for these samples came from [29].

In Figure 2, it can be seen that the SPS-125 sample had the highest nanoindentation and nanoindentation creep hardness in all samples, and also the smallest absolute percentage difference in the hardness between the indentation values and the creep values. It would appear that within the margin of error of this testing technique there is no measurable change in the SPS-125 sample between the nanoindentation hardness and nanoindentation creep hardness at 300 °C. Due to some difficulties the 500 °C data was not valid and is not included in the results. Results in Table 1 indicate that the SPS-125 sample has a creep exponent that is above 10 for both 300 and 500 °C. This suggests that the stress applied in the nanoindentation creep experiments is below the threshold stress needed to cause creep strain in the samples and is the reason for not observing a change in the hardness from the nanoindentation and nanoindentation creep experiments. This will be further expanded upon in the creep section of the discussion.

When evaluating the data in Table 2, the difference in hardness for sintered and pre-strained samples is larger at 500 °C than at 300 °C. In [7] the brittle to ductile transition temperature (BDTT) is reported to be in the range of 287-478 ºC for UO_2. As the 300 °C indents are at the beginning of this temperature range it would be expected that there would be a smaller difference in the nanoindentation hardness and nanoindentation creep hardness as compared with the 500 °C data. It would be expected that the 500 °C data would exhibit a larger difference because this testing condition is above the BDTT range.

When comparing the percentage decreases for the sintered, pre-strained and SPS-1.8 samples at 300 °C, the data indicated that the pre-strained and SPS-1.8 samples had significantly larger decreases in the hardness than the sintered sample. The decreases in hardness for the pre-strained and SPS-1.8 are 8.65 and 6.74 %, respectively, while the sintered sample decreased 2.48% at 300 °C. It is believed that the pre-strained and SPS 1.8 μm have larger decreases in hardness as compared with the sintered sample because of the pre-existing dislocations and other defects in the samples from the pre-strain or the SPS process. Regarding the latter, the literature suggests that samples produced through SPS have higher defect densities, such as dislocations, than conventionally produced material due to the high energy ball milling of the powder that occurs prior to the SPS [44, 45]. On the other hand, the regularly sintered UO_2 material would need to nucleate the dislocations prior to the deformation occurring.

Nanoindentation Creep

The small sample volumes (~1 μm depth, Figure 3) probed during the nanoindentation creep tests limited the volume of material sampled and, therefore, the number of microstructural features tested. This can become a specific issue when grain boundaries are part of the deformed region as is most likely the case in the fine-grained material. These limited grain boundaries in

the coarse-grained material make these tests similar to single crystal creep tests in $UO_{2,}$ as most of the deformation would be occurring inside the grains by dislocation motion instead of grain boundary sliding. The sampling of individual gains can cause an issue with anisotropy of properties as discussed above in the nanoindentation hardness section. In order to sample a random set of grains and get a statically average value at least 10 nanoindentation creep experiments were performed on each sample. In addition, the difference between the grain boundary density of the sintered sample and the SPS-125 can allow for possible evaluation of the effect of grain boundaries on the deformation.

The stress exponent (n) range for dislocation creep is 3-10 [31-36]. When the stress exponent is large (n > 10) it is typically explained by introducing a "threshold stress" below which creep cannot be measured [35, 36]. A review of the current literature shows two creep ranges proposed for $UO_{2,}$ which are based on the levels of stress required to initiate the deformation. In the low stress region, the stress exponent is 1. However, there are still some debates about this region and is explained by Coble diffusional and Harper-Dorn creep [18-25]. In the high stress region, the stress exponent is in the range of 4-5 and the dominant deformation mechanism is a diffusion-controlled dislocation creep process [18-25]. The data here indicated that the pre-strained and SPS-1.8 samples have stress exponents between 3-4 during the 500 °C nanoindentation creep measurements. This would suggest that the pre-strained and SPS-1.8 samples are both deforming by dislocation glide at these low temperature and high stress conditions.

The sintered sample has a higher stress exponent than the pre-strained and SPS-1.8 samples for the 500 °C tests: this could be due to the need to nucleate dislocations for the deformation process to occur as previously discussed. In other words, the diffusional dislocation creep cannot support the deformation process because there were insufficient dislocations available, as previously discussed in the nanoindentation hardness section. This need for nucleating dislocations was not present in the pre-strained and SPS-1.8 samples because the former sample had a pre-existing dislocation population due to the creep deformation before testing. The SPS-1.8 sample likely developed a high defect density as a result of the high energy ball milling of the powders before SPS [45,46]. The SPS-125 sample had a relatively large number of grain boundaries for the testing volume and the stress exponents measured here (~ 15) match well with literature values for high strain rate and high stress creep tests (16-20) [10, 24].

Sintered and Pre-strained Samples

The reasons for the increased creep rates for the pre-strained sample as compared with the sintered sample are believed to be the same as summarized in the nanoindentation hardness section, i.e., an increase in the defect density due to the deformation process at elevated temperature and that the plasticity of UO_2 is reduced at lower temperature because of the energetic barriers to dislocation nucleation [7]. The addition of dislocations nucleated during the high temperature deformation process provided the necessary minimum number of dislocations to allow plastic deformation to occur. This phenomenon can be seen in the difference in the stress exponents of the sintered and pre-strained samples at 300 ºC: at this temperature the sintered sample has a stress exponent that was greater than 10 while the pre-strained sample had a stress exponent ~ 8. This implies that the sintered sample had little to no creep occurring at 300 °C, while the pre-strained sample had some creep occurring by dislocation glide. It should be noted that at 500 °C the pre-strained sample still had a lower value for the stress exponent than

the sintered sample, which would infer that the dislocation nucleation process is still affecting the deformation of the UO_2 at 500 °C. While it is difficult to compare the stress exponent *n* of the sintered with literature values as most creep testing of UO_2 is performed at higher temperature (> 1000 ºC) and lower stress compared to these experiments, and under uniaxial load, the 500 ºC pre-strained values are comparably in the range of other macroscale creep experiments [18,19,25,47-50]. This could suggest that the brittle to ductile transition is indeed in the range suggested by [7] of 350-478 ºC for UO_2.

The SPS samples

The SPS-1.8 sample had *n* values lower than 10 at both 300 °C and 500 °C while the SPS-125 sample had *n* values that were greater than 10 at both 300 °C and 500 °C. Detailed microstructural analysis of the sample was not performed, but these creep results would suggest that the SPS process produced samples with higher defect densities, as described earlier, than the conventionally prepared samples, leading to increase creep rates when compared with the sintered sample. The pre-existing defects allowed for lower *n* values by providing the necessary dislocations for the deformation of the SPS-1.8 sample. In addition, in comparing the hardness values of the SPS-1.8 sample from [29] with the hardness values of the sintered sample it can be seen that that the SPS-1.8 sample also had a lower hardness than the sintered sample even with a smaller grain size.

When grain size changed from 1.8 μm to 125 nm the density of grain boundaries is increased, which was could be the underlying reason no measurable creep is observed in these experiments. The large *n* values for the SPS-125 sample at both 300 °C and 500 °C would suggest that these experiments are below the threshold stress to cause creep. This is not unexpected as literature has indicated that nanoceramics exhibit better mechanical properties because the nano sized grains produce a reduction of flaw size, structural homogenization, which leads to a reduction of residual stress levels, and barriers to dislocation motion because of the substantial increase in grain boundaries [51-54]. Due to the results of the SPS-1.8 sample one might speculate that the SPS-125 sample would also have a large density of defects and that grains boundaries are impeding their glide through the sample. However, the high density of grains boundaries in SPS-125 sample could act as defect sinks in the material [54]. This would lead to a lower dislocation density and possibly to a more pristine material in the grain interiors. In addition, these temperatures are not high enough for effective nucleation of dislocations at the boundaries for the deformation to occur. Furthermore, dislocations present or nucleated would have difficulties moving through the sample as they would be annihilated at grain boundaries. Grain boundary sliding is another potential deformation mechanism for UO_2. In the SPS-125 sample due to the high grain boundary density, it could be a possibility in these experiments. However, grain boundary sliding is usually seen at high temperatures and low strain rates [23-25, 55] as compared with the experiments here. The low temperatures here do not provide the diffusion activity needed to have effective grain boundary sliding. In addition, it usually leads to stress exponents of 1.5-2.5 that do not agree with the results here [55]. Most literature proposes that the deformation of UO_2 at lower temperatures is usually controlled by a Peierls mechanism [10, 24], which is also believed to be seen here. It would appear that stress has not reached the threshold leved needed to cause creep in the SPS-125 samples.

In comparing the SPS-125 and the sintered samples it can be seen that both had *n* values greater than 10 at 300 °C while the *n* value for the sintered sample went below 10 at 500 °C while the

SPS-125 stayed above 10. The reason for the difference is likely the density of grain boundaries in the tested volume of material. The tested volume in the sintered sample would have minimal grain boundaries allowing any dislocation nucleated to glide a relatively far distance when compared with the test volume. In addition, for the sintered sample there could be higher density of dislocations to start with as there are not as many grain boundaries to act as dislocation sinks. It has been observed that the density of grain boundaries in the test volume can affect the results as seen in literature [23-25, 29, 48, 50-54] with phenomena like the Hall-Petch effect and should be consider when evaluating the results.

Conclusions

This research demonstrates that nanoindentation based techniques can be successfully used to measure the mechanical properties of UO_2 samples with different microstructures. The results of this study also show that increasing the defect density of a UO_2 sample can decrease the creep stress exponent and hardness of these UO_2 samples at relatively low temperatures at and below the DBTT for UO_2. These results suggest the plasticity of UO_2 at lower temperatures could be hindered by the energetic barriers to dislocation nucleation. In addition, it is shown that UO_2 tested at high stress and low temperatures experiences creep that is consistent with dislocation glide as a creep mechanism. It was also observed that NC UO_2 did not exhibit creep during these experiments, potentially due to a very high threshold stress that was not reached during the tests.

The ability to measure the change in the properties of materials with different grain sizes as well as pre-strained and pristine materials illustrates that nanoindentation can be a valuable tool to measure the mechanical properties of materials using limited volumes. Additionally, because nanoindentation samples a small volume it can also be used to measure the difference in the mechanical properties along the length of a spent fuel pellet. This could allow for the investigation of the mechanical properties in different regions determined by the varying identifiable microstructures, which is not possible with conventional macroscale mechanical testing due to the propensity of the pellets to crack, the high level of radioactivity, and the size of the specimen needed for macroscale mechanical testing. The use of this technique on neutron irradiated fuel could greatly decrease the post irradiation examination time while allowing more information to be gathered from a single specimen.

Conflict of Interes

The authors have no conflict of interest.

Acknowledgments

This work was supported by the U.S. Department of Energy, Office of Nuclear Energy under the Nuclear Engineer University Program (award numbers: DE-NE0008440 and DE-NE-000067000). Nano-indentation experiments were supported through a NSUF RTE award (award number: 17-849) under DOE Idaho Operations Office Contract DE-AC07-051D14517 as part of a Nuclear Science User Facilities Experiments.

References

[1] D. Olander “Nuclear Fuels-Present and future” J. Nucl. Mater. 289 (2009) 1-22

[2] N. Marchal, C. Campos, C. Garnier “ Finite element simulation of Pellet-Cladding Interaction (PCI) in nuclear fuel rods” Comput. Mater. Sci. 45 (2009) 821-826ss

[3] H.C. Kim, S.K. Seo, S.U. Lee, Y.S. Yang “Development of NUFORM3D module with FRAPCON3.4 for simulation of pellet-cladding mechanical interaction” Nucl. Eng. Deg. 318 (2017) 61-71

[4] Y. Deng, Y. Wu, B. Qiu, D. Zhang, M. Wang, W. Tian, S. Qiu, G.H. Su “Development of a new Pellet-Clad Mechanical Interaction (PCMI) model and its applications in ATFs” Annals Nucl. Energy 104 (2017) 146-156

[5] B. Michel, J. Sercombe, G. Thouvenin, R. Chatelet “3D fuel cracking modelling in pellet cladding mechanical interaction” Eng. Fract. Mech. 75 (2008) 3581-3598

[6] J.F. Byron, “Yield and flow of polycrystalline uranium dioxide” J. Nucl. Mater. 27 (1968) 48-53

[7] R.J. Keller, T.E. Mitchell, A.H. Heuer, “Plastic deformation in nonstoichiometric UO2+x single crystals—1. Deformation at low temperatures” Acta Metallurgica 36 (1988) 1061-1071

[8] K.C. Radford, G.R. Terwilliger “Compressive Deformation of Polycrystalline UO2” J. Am. Ceram. Soc. 58 (1975) 274-278

[9] A.G. Evans, R.W. Davidge “The strength and fracture of stoichiometric polycrystalline UO2” J. Nucl. Mater. 33 (1969) 249-260

[10] R.F. Canon, J.T.A. Roberts, R.J. Beals “Deformation of UO2 at High Temperatures” J. Am. Ceram. Soc. 54 (1971) 105-112

[11] D. Frazer, B. Shaffer, K. Roney, H. Lim, B. Gong, P. Peralta, P. Hosemann “Small-scale mechanical testing of UO2” Transactions of the American Nuclear Society 116 (2017) 485-487

[12] D. Frazer, B. Shaffer, K. Roney, H. Lim, B. Gong, P. Peralta, P. Hosemann “Elevated Temperature Nanoindentation Testing of UO 2 ” Transactions of the American Nuclear Society 117 (2017) 623-624

[13] K.A. Terrani, M. Balooch, J.R. Burns, Q.B. Smith “Young’s modulus evaluation of high burnup structure in UO2 with nanometer resolution” J. Nucl. Mater. 508 (2018) 33-39

[14] R. Skelton, A.M. Walker “Peierls-Nabarro modeling of dislocations in UO2” J. Nucl. Mater. 495 (2017) 202-210

[15] L. Portelette, J. Amodeo, R. Madec, J. Soulacroix, T. Helfer, B. Michel “Crystal viscoplastic modeling of UO2 single crystal” J. Nucl. Mater. 510 (2018) 635-643

[16] A.V. Lunev, A.Yu. Kuksin, S.V. Starikov, “Glide Mobility of the ½[110](001) edge dislocation in UO2 from molecular dynamics simulation” Int. J. Plast. 89 (2017) 85-95

[17] D. Frazer, P. Hosemann “Plasticity of UO2 quantified and understood via Elevated Temperature micro compression testing” J. Nucl. Mater. 525 (2019) 140-144

[18] X. Iltis, N. Gey, C. Cagna, A. Hazotte, Ph. Sornay "Microstructural evolution of uranium dioxide following compression creep tests: An EBSD and image analysis study" J. Nucl. Mater. 456 (2015) 426-435

[19] X. Iltis, M.B. Saada, H. Mansour, N. Gey, A. Hazotte, N. Maloufi "A new characterization approach for studying relationships between microstructure and creep damage mechanisms of uranium dioxide" J. Nucl. Mater. 474 (2016) 1-7

[20] M.S. Seltzer, A.H. Clauer, B.A. Wilcox "The influence of stoichiometry on compression creep of polycrystalline UO_{2+x}" J. Nucl. Mater. 44 (1972) 331-336

[21] M.S. Seltzer, A.H. Clauer, B.A. Wilcox "The influence of stoichiometry on compression creep of uranium dioxide single crystals" J. Nucl. Mater. 44 (1972) 43-56

[22] W.M. Armstrong, A.G. Causey, W.R. Sturrock "Creep of Single-Crystal UO_2" J. Nucl. Mater. 19 (1966) 42-49

[23] F. Dherbey, F. Louchet, A. Mocellin, S. Leclercq "Elevated temperature creep of polycrystalline uranium dioxide: from microscopic mechanisms to macroscopic behavior" Acta Materialia 50 (2002) 1495-1505

[24] M. Salvo, J. Sercombe, J.C. Menard, J. Julien, T. Helfer, T. Desoyer "Experimental characterization and modelling of UO_2 behavior at high temperature and high strain rates" J. Nucl. Mater. 456 (2015) 54-67

[25] O.A. Ruano, J. Wolfenstine, J. Wadsworth, O.D. Sherby "Harper-Dorn and power law creep in Uranium dioxide" Acta Metall. Mater. 39 (1991) 661-668

[26] V.V. Rondinella, T. Wiss "The high burn-up structure in nuclear fuel" Mater. Today 13 (2010) 24-32

[27] H. Xiao, C. Long "Modeling of Pore Coarsening in the Rim Region of High Burn-up UO_2 fuel" Nucl. Eng. Tech. 48 (2016) 1002-1008

[28] F. Cappia, D. Pizzocri, M. Marchetti, A. Schubert, P. Van Uffelen, L. Luzzi, D. Papioannou, R. Macian-Juan, V.V. Rondinella "Microhardness and Young's modulus of high burn-up UO_2 fuel" J. Nucl. Mater. 479 (2016) 447-454

[29] B. Gong, D. Frazer, T. Yao, P. Hosemann, M. Tonks, J. Lian, "Nano-and micro-indentation testing of sintered UO_2 fuel pellets with controlled microstructure and stoichiometry" J. Nucl. Mater. 516 (2019) 169-177

[30] M. Cologna, V. Tyrpekl, M. Ernstberger, S. Stohr, J. Somers, " Sub-micrometre grained UO_2 pellets consolidated from sol gel beads using spark plasma sintering (SPS)" Ceram. Intern. 42 (2016) 6619-6623

[31] S.N.G. Chu, J.C.M. Li, "Impression creep; a new creep test" 11 (1977) 2200-2208

[32] F. Li, Y. Xie, M. Song, S. Ni, S. Guo, X. Liao, "A detailed appraisal of the stress exponent used for characterizing creep behavior in metallic glasses" Materials Science and Engineering: A 654 (2016) 53-59

[33] P. Sudharashan Phani, W.C. Oliver "A direct comparison of high temperature nanoindentation creep and uniaxial creep measurements for commercial purity aluminum" acta materialia 111 (2016) 31-38

[34] A.F. Bower, N.A. Fleck, A. Needleman, N. Ogbonna "Indentation of a power law creeping solid" Proc. R. Soc. London Ser. A, 441 (1993) 97-124

[35] C. Su, E.G. Herbert, S. Sohn, J.A. LaManna, W.C. Oliver, G.M. Pharr "Measurement of power-law creep parameters by instrumented indentation methods" J. of the mechanics and physics of solids 61 (2013) 517-536

[36] J. Dean, A. Bradbury, G. Aldrich-Smith, T.W. Clyne "A procedure for extracting primary and secondary creep parameters from nanoindentation data" Mechanics of Materials 65 (2013) 124-134

[37] V.G. Baranov, A.V. Lunev, A.V. Tenishev, A.V. Khlunov, "Interaction of dislocations in UO_2 during high burn-up structure formation" J. Nucl. Mater. 444 (2014) 129-137

[38] J. Spino, J. Cobos-Sabate, F. Rousseau "Room-temperature microindentation behavior of LWR-fuels, part 1: fuel microhardness" J. Nucl. Mater. 322 (2003) 204-216

[39] D. Frazer, C.P. Deck, P. Hosemann "High Temperature Nanoindenation of SiC/SiC composites" JOM 72 (2020) 139-144

[40] W.C. Oliver, G.M. Pharr "An improved technique for determining hardness and elastic modulus using load and displacement sensing indentation experiments" J. Mater. Res. 7 (1992) 1564-1583

[41] C.S. Yust, C.J. McHargue "Dislocation substructures in deformed uranium dioxide single crystals" 31 J. Nucl. Mater. (1969) 121-137

[42] P. Fossati, L.V. Brutzel, B. Devincre "Molecular dynamics simulation of dislocations in uranium dioxide" 443 (2013) 359-365

[43] C.S. Yust, J.T.A. Roberts "On the observation of lattice and grain boundary dislocation in UO_2 deformed at high temperatures" 48 J. Nucl. Mater. (1973) 317-329

[44] A.H. Heuer, R.J. Keller, T.E. Mitchell *Deformation processes in Minerals, Ceramics and Rocks Chapter 15: On the slip systems in uranium dioxide* D.J. Barber, P.G. Meredith Unwin Hyman Ltd.

[45] J.D. Hahn, F. Wu, P. Bellon "Cr-Mo Solid Solutions Forced By High-Energy Ball Milling" Metall. Mater. Trans. A 35A (2004) 1105-1111

[46] C. Suryanarayana "Mechanical alloying and milling" Prog. Mater. Sci. 46 (2001) 1-184

[47] W.M. Armstrong, W.R. Irvine, R.H. Martinson "Creep deformation of stoichiometric uranium dioxide" 7 J Nucl. Mater. (1962) 133-141

[48] J.C. Gao, L.F. Wang, Y. Wang, S.F. Wu "High-temperature creep properties of uranium dioxide pellet" 20 Trans. Nonferr. Metals Soc. China (2010) 238-242

[49] M. Ben Saada, N. Gey, B. Beausir, X. litis, H. Mansour, N. Maloufi "Sub-boundaries induced by dislocation creep in uranium dioxide analyzed by advanced diffraction and channeling electron microscopy" 133 Mater. Chara. (2017) 112-121

[50] F.A. Mohamed, M.S. Soliman "On the creep behavior of uranium dioxide" 79 J. Nucl. Mater. (1979) 143-153

[51] W.D. Callister. Fundamentals of Materials Science and Engineering, 2nd ed. Wiley & Sons. pp. 252.

[52] I.A. Ovid'ko, A.G. Sheinerman, E.C. Aifantis "Stress-driven migration of grain boundaries and fracture processes in nanocrystalline ceramics and metals" 56 Acta Metaer. (2008) 2718-2727

[53] S.V. Bobylev, A.K. Mukherjee, I.A. Ovid'ko "Emission of partial dislocation from amorphous intergranular boundaries in deformed nanocrystalline ceramics" 60 Scripta Mater. (2009) 36-39

[54] Mechanical Properties of Nanocrystalline Materials editor James C.M. Li Pan Stanford publishing Pte. Ltd. 2011

[55] J.T.A. Roberts "Mechanical Equation of state and high-temperature deformation (>0.5T_m) of uranium dioxide" Acta metallurgica 22 (1974)

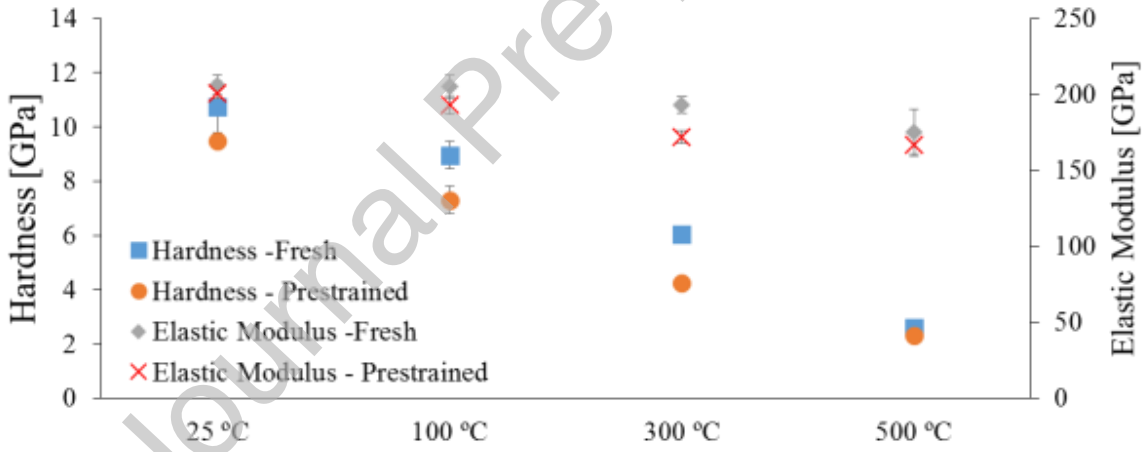

Figure 1: The elevated temperature nanoindentation results on Fresh (Sintered) and Prestrained samples. The error bars are the standard deviation of the all of the results. A minimum of 15 indents per test condition were performed.

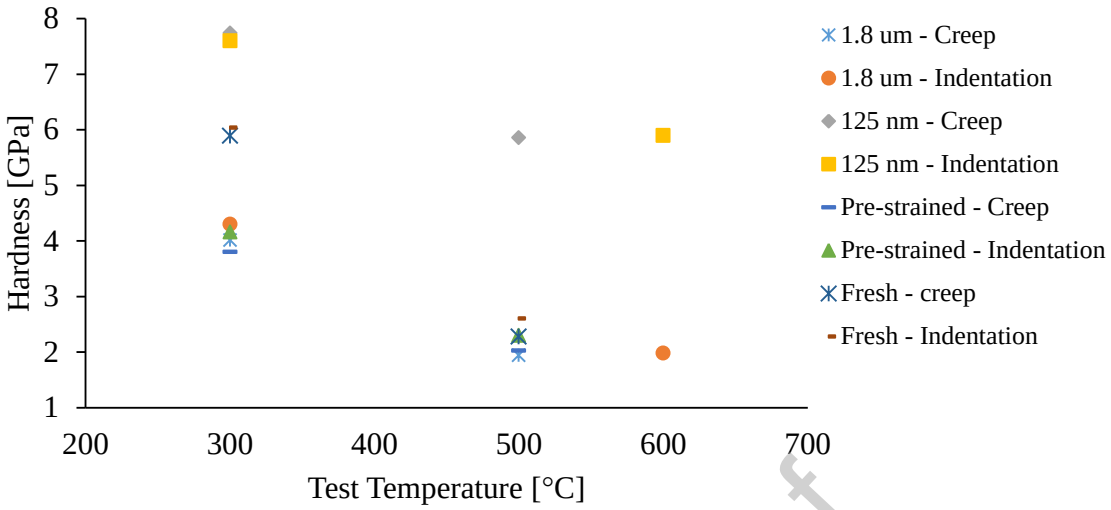

Figure 2: A plot showing the hardness values of 4 different samples of UO_2 depending on the testing method used.

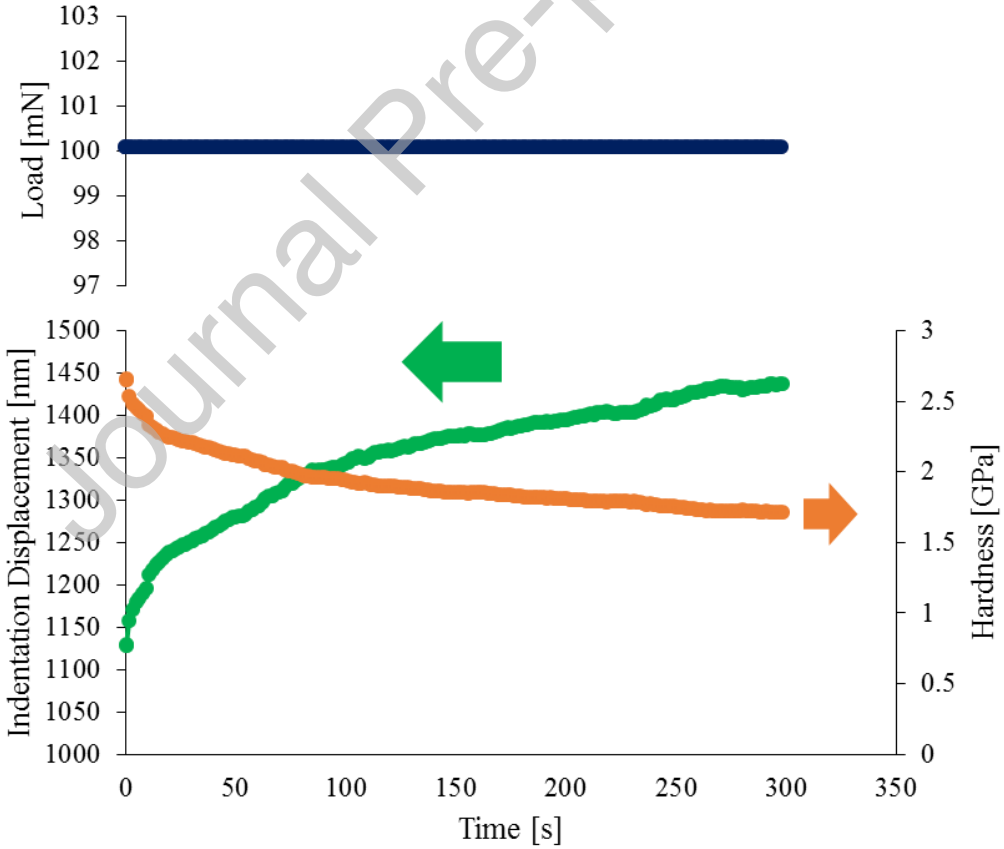

Figure 3: Data from a 500 °C nanoindentation creep test for the SPS-1.8 sample. The top plot shows the load for the tes as a function of time, which was 100.8 mN. The bottom plot shows the displacement of the indenter during the hold and the decrease in the measured hardness of the material during the hold.

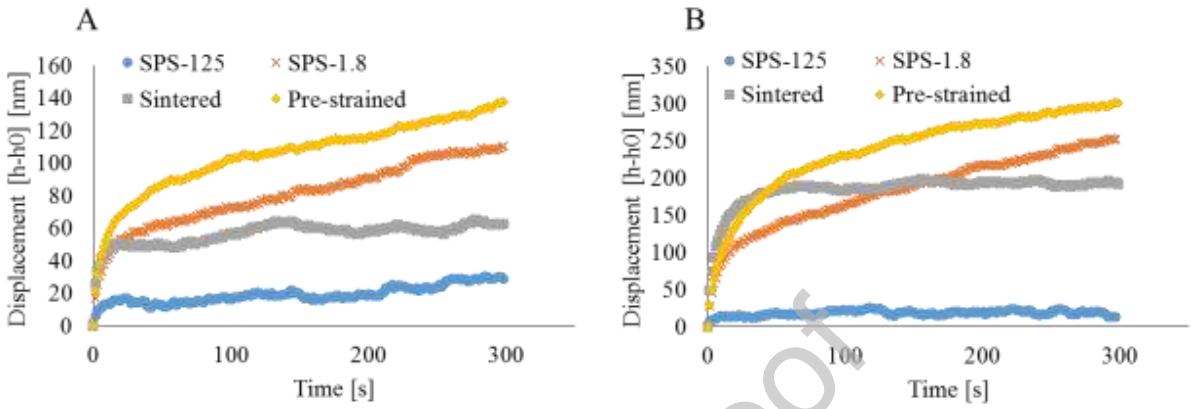

Figure 4: Representative creep curves of the four different samples tested. A) 300 °C B) 500 °C.

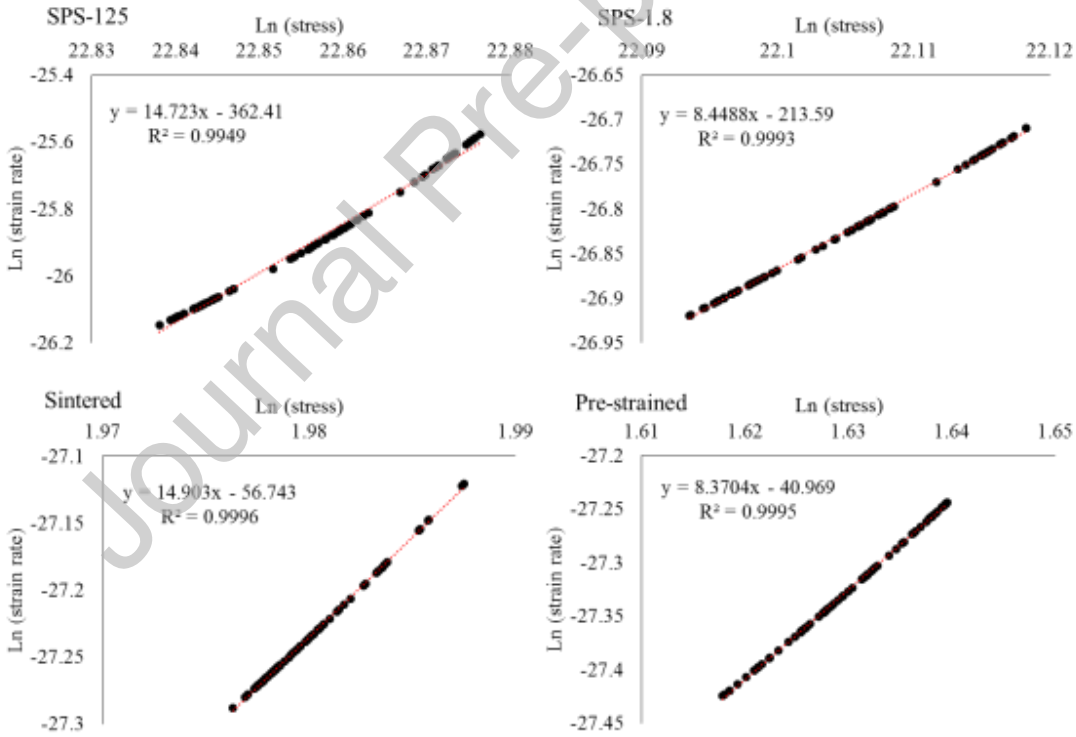

Figure 5: Representative ln(strain rate) versus ln(stress) curves for all fours samples at 300 °C.

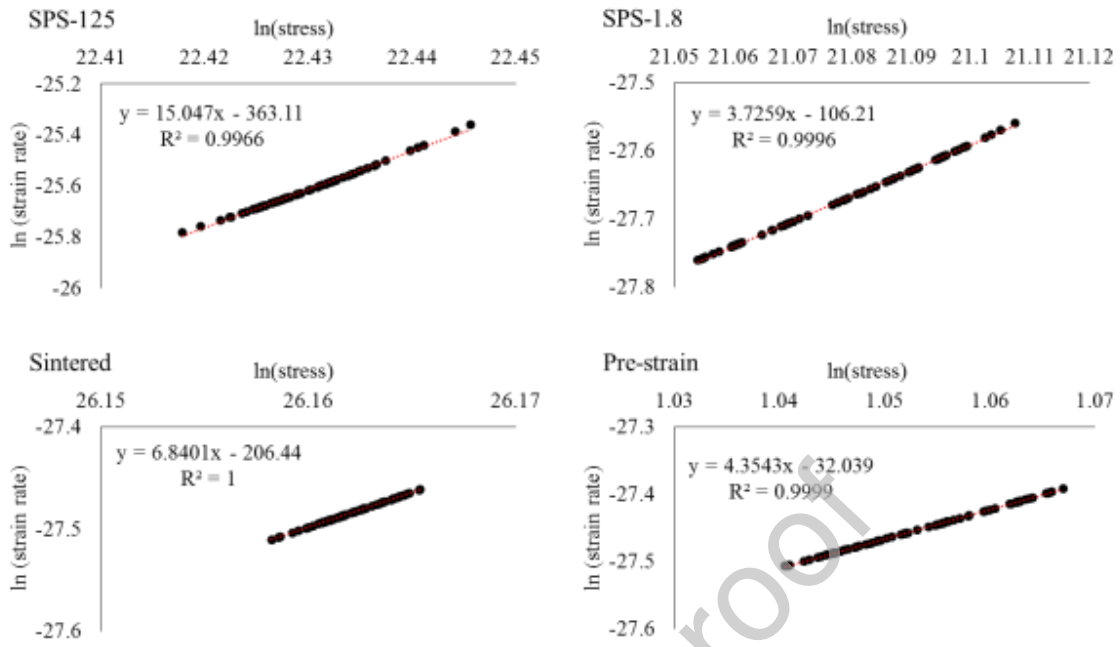

Figure 6: Representative ln(strain rate) versus ln(stress) curves for all four samples at 500 °C.

Table 1: Stress Exponents for the nanoindentation creep experiments at 300 and 500 °C. The error is the standard deviation of the results. A minimum of 10 nanoindentation creep experiments were performed for each condition.

Sample	1 (Sintered)	2 (prestrained)	3 (SPS 1.8 µm)	4 (SPS 125 nm)
300 ºC	16.1 ± 3.2	8.1 ± 0.4	8.7 ± 0.8	14.5 ± 3.0
500 ºC	6.9 ± 1.3	4.4 ± 0.3	3.5 ± 0.8	16.0 ± 5.0

Table 2: The hardness values of the 4 different samples from nanoindentation and nanoindentation creep experiments. The percentage decrease in hardness is also shown.

	Sintered 300 °C	*Sintered 500 °C*	*Prestrained 300 °C*	*Prestrained 500 °C*	*SPS 1.8 µm 300 °C*	*SPS 125 nm 300 °C*
Nanoindentation - Hardness [GPa]	*6.0*	*2.6*	*4.2*	*2.3*	*4.3*	*7.6*
Nanoindentation Creep – Hardness [GPa]	*5.9*	*2.3*	*3.8*	*2.0*	*4.0*	*7.7*
% Decrease in Hardness	*2.48*	*12.31*	*8.65*	*11.74*	*6.74*	*-1.84*